inorganics

MDPI

Article

ZnO and ZnO/Ce Powders as Tribocatalysts for Removal of Tetracycline Antibiotic

Dobrina Ivanova [1], Hristo Kolev [2], Bozhidar I. Stefanov [3] and Nina Kaneva [1,*]

[1] Laboratory of Nanoparticle Science and Technology, Department of General and Inorganic Chemistry, Faculty of Chemistry and Pharmacy, University of Sofia, 1164 Sofia, Bulgaria; dobrina.k.ivanova@gmail.com
[2] Institute of Catalysis, Bulgarian Academy of Sciences, Acad. G. Bonchev St., bl. 11, 1113 Sofia, Bulgaria; hgkolev@ic.bas.bg
[3] Department of Chemistry, Faculty of Electronic Engineering and Technologies, Technical University of Sofia, 8 Kliment Ohridski Blvd, 1756 Sofia, Bulgaria; b.stefanov@tu-sofia.bg
* Correspondence: nina_k@abv.bg

Abstract: Research on tribocatalysis, which involves the triboelectric effect, is based on the concept that friction between dissimilar materials can generate charges capable of initiating catalytic reactions. This phenomenon holds significant potential for the degradation of wastewater contaminants in the environment. In this study, pure and Ce-modified (2 mol%) ZnO powders were investigated as tribocatalysts for the degradation of doxycycline (DC), a tetracycline antibiotic, in the absence of light. The research demonstrates that friction between the catalyst, the beaker, and the polytetrafluoroethylene (PTFE) magnetic rod induces charge transfer at their interfaces, leading to the breakdown of pollutants. Additionally, doxycycline degradation was observed at three different stirring speeds (100, 300, and 500 rpm). The results confirmed the tribocatalytic effect, showing that DC degradation increases with higher stirring speeds. Using ZnO and ZnO/Ce powders, maximum degradations of 80% and 55%, respectively, were achieved in 24 h at a stirring speed of 500 rpm. The findings of this study suggest that these samples can effectively degrade contaminants in water through the application of mechanical energy.

Keywords: tribocatalysis; ZnO/Ce powders; tetracycline antibiotic

check for updates

Citation: Ivanova, D.; Kolev, H.; Stefanov, B.I.; Kaneva, N. ZnO and ZnO/Ce Powders as Tribocatalysts for Removal of Tetracycline Antibiotic. *Inorganics* **2024**, *12*, 244. https://doi.org/10.3390/inorganics12090244

Academic Editors: Tobias Krämer and Geun-Ho Han

Received: 28 July 2024
Revised: 26 August 2024
Accepted: 4 September 2024
Published: 5 September 2024

Correction Statement: This article has been republished with a minor change. The change does not affect the scientific content of the article and further details are available within the backmatter of the website version of this article.

Copyright: © 2024 by the authors. Licensee MDPI, Basel, Switzerland. This article is an open access article distributed under the terms and conditions of the Creative Commons Attribution (CC BY) license (https://creativecommons.org/licenses/by/4.0/).

1. Introduction

Wastewater treatment is a critical aspect of human society's development [1–3]. Several approaches exist for treating sewage, including photocatalysis [4–8], biodegradation [9], and adsorption [10–12]. While these methods are effective, each has inherent drawbacks. Chemical precipitation [13] can lead to secondary pollution, electrochemical methods are power-intensive and economically burdensome, biodegradation requires a prolonged degradation cycles [14,15], and photocatalysis suffers from low solar energy utilization rates and the easy recombination of photogenerated carriers [16–18]. Additionally, adsorption selectively adsorbs pollutants without decomposing them [19]. Therefore, it is essential to explore more effective and sustainable wastewater treatment techniques, such as tribocatalysis, based on the utilization of mechanical and frictional energy, which, like light energy, may be supplied via green energy sources widely used in industrial production.

Tribocatalysis is a mechano-electrochemical advanced oxidation process which employs the triboelectric effect—generating charges upon the frictional energy transfer between dissimilar surfaces, which in turn may react with water molecules, dissolved oxygen, and hydroxide ions in the aqueous phase, generating highly active free radicals, such as $O_2^{\bullet -}$ and $OH^{\bullet}$. These radicals are effective in pollutant removal due to their potent oxidizing properties. Although tribocatalysis, or frictional catalysis, is still relatively unexplored in the literature, it has already garnered significant interest. Lei et al. [20] demonstrated that $BiOIO_3$ could catalyze the degradation of Rhodamine B (RhB) by over 90% in less than

six hours by converting frictional energy into electrical charges and, subsequently, chemical energy. Another study by Gaur et al. [21] used calcium copper titanate nanoparticles with strong tribocatalytic activity to degrade cationic organic dyes such as RhB and MB. However, research on the application of tribocatalysis in the degradation of pharmaceutical products remains limited.

Antibiotics released into the environment from sources such as livestock excrement, hospitals, households, and pharmaceutical industries are contributing to the proliferation of bacterial strains resistant to current treatments, posing challenges for ecosystem management [22,23]. After ingestion, antibiotics undergo metabolism, but prolonged exposure can lead to mutagenic effects, nephropathy, spermatogenesis effects, arthropathy, photosensitivity, and damage to the central nervous system in organisms [24]. Thus, pollutants in wastewater must be fully mineralized. Doxycycline is an example of such an antibiotic.

Doxycycline (DC), a member of the tetracycline antibiotic family, is used in both human and veterinary medicine to treat Gram-positive and Gram-negative bacteria [25]. It consists of three functional groups: dimethylamine, tricarbonyl amide, and phenolic diketone [26]. Due to its chemical stability, DC is not biodegradable [26,27], making advanced oxidation processes a reliable method for breaking down these persistent pollutants.

This study investigates the degradation of doxycycline through tribocatalysis (friction catalysis) in the absence of light. We utilized hydrothermal ZnO and ZnO/Ce powders as tribocatalysts and evaluated their properties under stirring conditions. Factors, such as cerium ion incorporation, magnetic stirring speed, and the recyclability of modified samples were assessed to understand their influence on tribocatalysis in the degradation of tetracycline antibiotics.

2. Results and Discussion

2.1. Characterization of the Pure and Cerium Modified ZnO Powders

ZnO and ZnO/Ce powders were subjected to X-ray diffraction (XRD) analysis to investigate the crystal structure of the samples (Figure 1). Intense diffraction peaks at 2θ = 31.94°, 34.67°, 36.51°, 48.23°, 56.84°, 63.22°, 67.53°, and 68.18° indicate that the pure semiconductor is in the hexagonal wurtzite crystalline phase. These peaks correspond to the lattice plane orientations with *hkl* values of (100), (002), (101), (102), (110), (103), (112), and (201) [28].

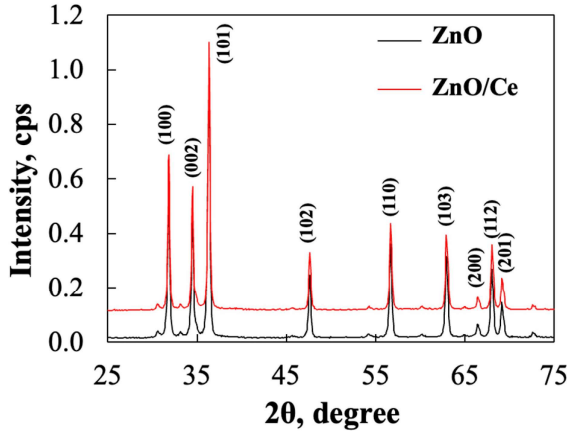


Figure 1. XRD patterns of ZnO and ZnO/Ce powders.

The peak locations are consistent with the data from JCPDS Card No. 36-1451, confirming the absence of impurities or phase changes in the crystalline structure of the powder. The strong, sharp peaks in the XRD patterns of both pure and ZnO/Ce samples indicate a high degree of crystallinity. The nearly identical XRD patterns of the ZnO catalyst before and after cerium modification suggest that the crystal structure remains unchanged [29]. The absence of a distinct ceria phase in the modified ZnO composite can be attributed to

its low concentration (2 mol%). Notably, ZnO modified by Ce shows a slight increase in the average crystallite size compared to pure ZnO, as determined by the Scherrer equation using the main peak (101). The modified ZnO catalyst has crystallite sizes of about 44 nm, while pure ZnO has a size of 37 nm. The XRD data demonstrate that the addition of cerium ions (2 mol%) does not significantly alter the crystal size. The crystalline lattice parameters remain unchanged after modification: ZnO (a, b = 3.250 Å; c = 5.206 Å) and ZnO/Ce (a, b = 3.248 Å; c = 5.205 Å). Powders modified with cerium ions retain their hexagonal wurtzite structure, as indicated by the calculated lattice parameters, which closely resemble those of ZnO.

Additionally, when the microstrain of the powders is computed using the c-axis lattice parameter, a positive value indicating tensile strain is observed. The tensile strain in the modified sample (7.33×10^{-4} a.u.) is slightly lower than that in ZnO (8.57×10^{-4} a.u.).

Scanning electron microscopy (SEM) was used to analyze the microstructure and morphology of the pure and modified samples (Figure 2). The SEM images revealed that the ZnO sample contained particles of various shapes. According to the images, the average particle size for ZnO was 0.25 µm, while for Ce-modified samples, it was approximately 0.5 µm. The SEM analysis indicates that morphology is not significantly affected by the Ce-modification, due to the low treatment temperature (100 °C).

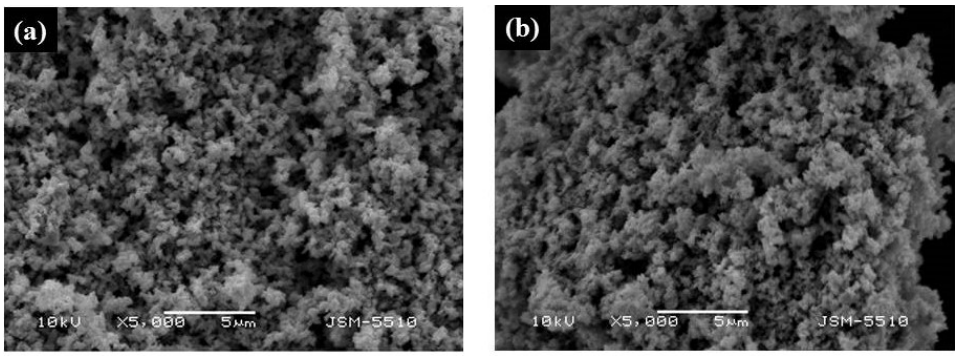


Figure 2. SEM images of (**a**) pure and (**b**) Ce-modified ZnO powders.

Energy-dispersive X-ray spectroscopy (EDS) was used to determine the presence of Zn, O, and Ce in the modified ZnO/Ce powder (Figure 3). Peaks representing zinc, oxygen, and cerium can be observed in the spectrum. It was found that Ce has a weight percentage of approximately 3 wt.%. The high purity of the initial ZnO is supported by the absence of impurity peaks in the EDS spectrum (Figure 3a). The mapping data in Figure 3b show that cerium is uniformly distributed across the ZnO surface.

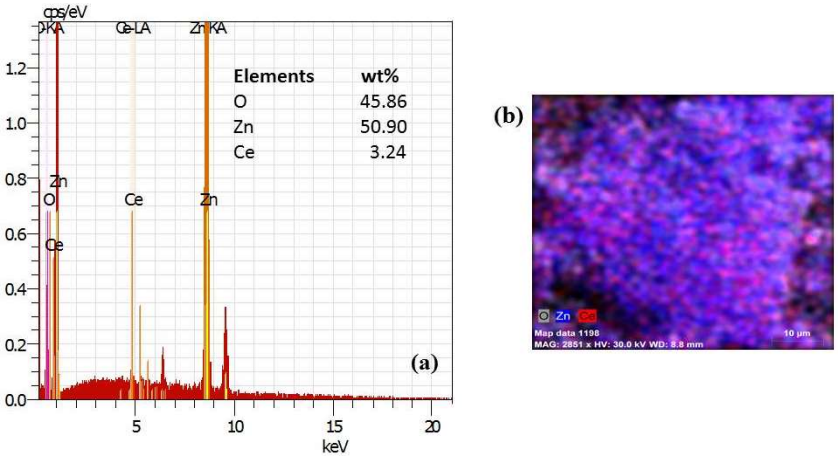


Figure 3. (**a**) EDS spectra of ZnO powder modified with cerium ions (2 mol%); (**b**) mapping surface data for ZnO/Ce powder.

Additionally, transmission electron microscopy (TEM) was used to observe the shape and location of the ceria phase on the ZnO surface. The resulting micrographs are shown in Figure 4. The TEM images confirm that the tribocatalysts consist of polycrystalline agglomerates approximately 0.25 μm in diameter, consistent with the SEM analysis, representing the ZnO phase (Figure 4a). The ZnO tribocatalyst was covered by the Ce-oxide phase, visible as surface-bound particles approximately 10 nm in diameter in the higher magnification images (Figure 4b). These images also reveal an interplanar spacing of 0.27 nm, consistent with the (100) plane of CeO_2 [30].

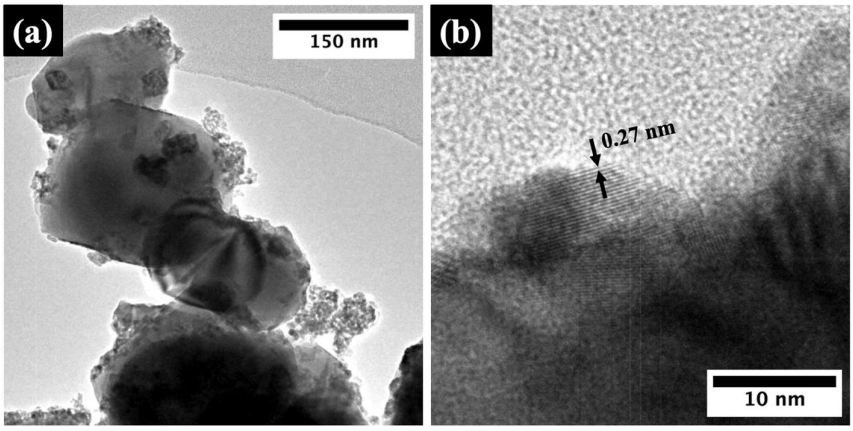


Figure 4. TEM micrographs of ZnO/Ce powder at (**a**) low and (**b**) high magnification.

The chemical states of the pure ZnO and ZnO/Ce tribocatalysts were analyzed using X-ray photoelectron spectroscopy (XPS). The high-resolution XPS spectrum of the Zn 2p core-level region of pristine ZnO (Figure 5a) shows a peak at a binding energy (BE) of 1021.7 eV, corresponding to Zn $2p_{3/2}$, along with an accompanying peak associated with $2p_{1/2}$ at approximately 1044.7 eV. In the ZnO/Ce sample (Figure 5c), this peak remains largely unchanged, indicating no significant interaction between the precursor and substrate. The O 1s core level region, depicted in Figure 5b, was deconvoluted to reveal XPS doublet peaks at 530.3 eV and 531.6 eV, corresponding to lattice oxygen and extraneous (non-lattice and/or oxygen vacancies) oxygen in wurtzite ZnO [31]. For the ZnO/Ce modification, the Ce 3d core level region (Figure 5e) displays three sets of peaks: two well-separated triplets peaking at 882.2 eV and 898.1 eV, along with a Ce^{4+}-satellite peak at 916.5 eV. These peaks correspond to the Ce $3d_{5/2}$ and Ce $3d_{3/2}$ core levels and are consistent with the formation of Ce(IV) oxide [32], indicating that the Ce^{3+} precursor was oxidized during preparation. Additionally, deconvolution of the O 1s region for the ZnO/Ce sample (Figure 5d) revealed a new low-intensity component at 529.5 eV (~6 at.%), which aligns with the formation of CeO_2. The decreased intensity of the 531.7 eV peak, compared to the pure ZnO sample, is associated with oxygen vacancies and/or non-lattice oxygen in the ZnO structure, consistent with observations in other CeO_x/ZnO nanocomposites [33]. The peak at 530.5 eV is again ascribed to the oxygen bonded with Zn, while the peak at 532.7 eV is associated with adsorbed water. The overall Ce(IV) concentration was determined to be 2.61 at.% (0.44 times less the oxygen associated with Ce-O bonds, close to the expected 0.5 ratio in CeO_2), which is consistent with the full incorporation of the approximately 2 mol% cerium precursor used to functionalize the tribocatalytic ZnO/Ce nanocomposite.

Raman spectroscopy was used to confirm the phase composition of the ZnO materials, and Figure 6 shows the resulting spectra. The E_2(high)-E_2(low) mode of ZnO, the E_2(high) mode, and the $2A_1$(low) + $2E_2$(low) broad band, correspond to the most intense Raman bands in all cases, appearing at 331, 439, and 1154 cm^{-1}, respectively [34]. These results support the presence of wurtzite ZnO and do not indicate any significant alteration of the primary tribocatalyst component as a result of functionalization.

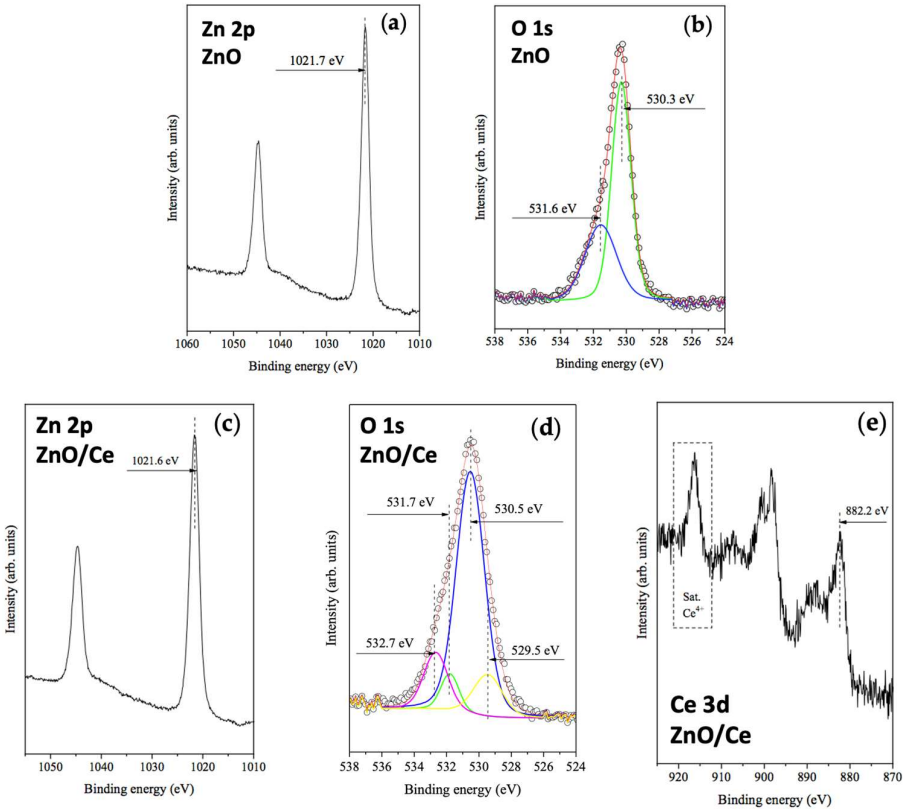


Figure 5. XPS spectra of ZnO and Ce-modified ZnO powders showing (**a**) Zn 2p region in pure ZnO; (**b**) O 1s region in pure ZnO; (**c**) Zn 2p region in ZnO/Ce; (**d**) O 1s region in ZnO/Ce; (**e**) Ce 3d region in ZnO/Ce.

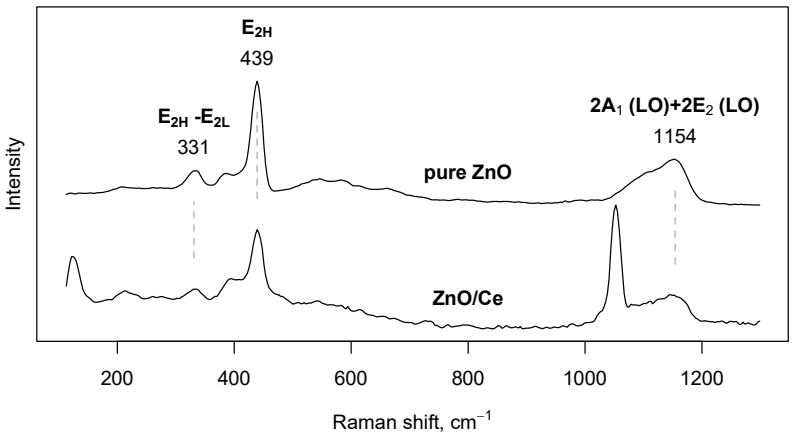


Figure 6. Raman spectra of pristine ZnO and ZnO/Ce powders.

2.2. Tribocatalysis for the Degradation of Doxycycline via ZnO and ZnO/Ce Powders

The tribocatalytic activity of ZnO and ZnO/Ce powders was investigated by the degradation of the antibiotic doxycycline (DC) in darkness, using a magnetic stirrer with a PTFE magnetic bar at 300 rpm. All friction tests employed the same drug concentration (15 mg/L). The concentration of the drug solution was determined by measuring the distinctive absorbance of the DC molecule at a wavelength of 275 nm.

As shown in Figure 7, the concentration of the pollutant only slightly decreases when no catalyst is used and no stirring is applied. This result demonstrates that the tribocatalytic process is not significantly impacted by the friction between the glass beaker and the magnetic bar. Degradation of doxycycline is only observed in the presence of

ZnO and ZnO/Ce tribocatalysts. After 24 h of magnetic stirring, the concentration of DC gradually decreased, signifying the degradation of the drug.

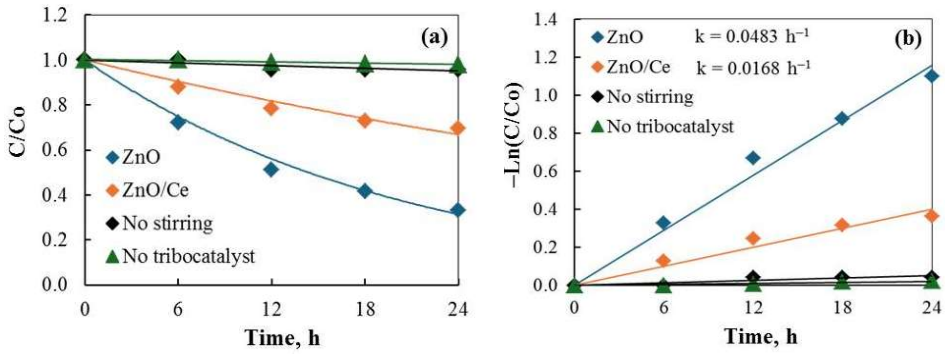


Figure 7. (**a**) Decomposition of antibiotic via ZnO and ZnO/Ce powder using magnetic stirring 300 rpm; (**b**) kinetic fitting.

Figure 7a illustrates the tribocatalytic decomposition of the DC solution using pure and Ce-modified ZnO powders that were annealed at 100 °C. The degradation results confirm the tribocatalytic action, with 66.67% and 30.42% of the drug being degraded by the ZnO and ZnO/Ce powders, respectively, after a 24 h friction period.

The ZnO/Ce powder exhibits lower catalytic efficiency compared to pure ZnO. The trend is corroborated by the rate constant values (Figure 7b), calculated using the equation $\ln(C_t/C_0) = -kt$. The ZnO sample demonstrates a higher reaction rate (k = 0.0483 h^{-1}) compared to the cerium-modified sample (k = 0.0168 h^{-1}).

A possible diagram of the tribocatalysis principle is depicted in Figure 8. Positive (q^+) and negative (q^-) charges are produced on the surfaces of the ZnO powders and the PTFE stirring rod when the ZnO catalyst is stirred and subjected to friction [35]. ZnO, excited by friction, generates positive and negative charges. Triboelectrically generated electric charges can also achieve DC decomposition, similar to photocatalytic drug decomposition based on photogenerated carriers. Superoxide radicals ($O_2^{\bullet -}$) are produced when oxygen molecules react with negative charges, while the positive charges on the surface of the ZnO powders are released into the water, producing active $OH^{\bullet}$ radicals [35–38]. These radicals further break down the antibiotic tetracycline into inorganic compounds like carbon dioxide and water. Other studies have found that the presence of Ce ions in the structure of ZnO photocatalysts may act as recombination centers for photogenerated charges via electron trapping, leading to energy loss [37]. It is plausible that a similar mechanism could be operating in the ZnO/Ce tribocatalysts in this study. In the case of cerium, fewer positive and negative charges are produced on the surface of the modified sample and the PTFE rod, resulting in fewer active radicals and a slower degradation rate of the drug.

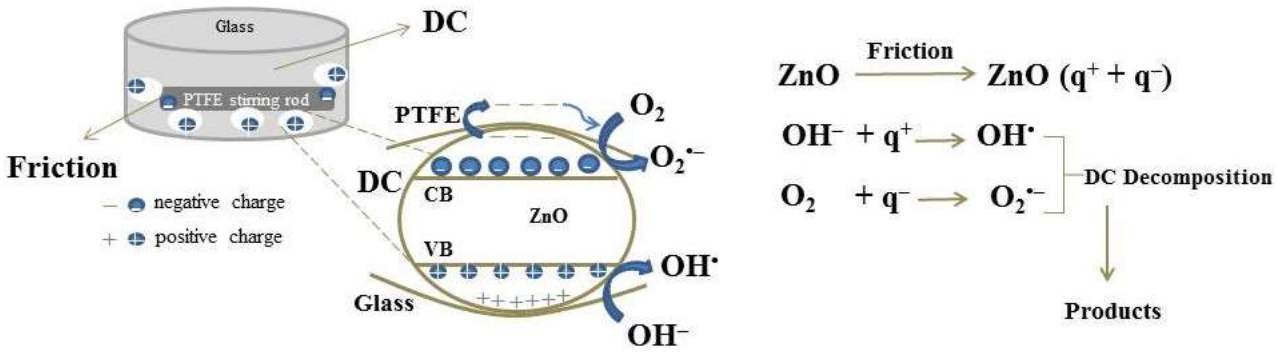


Figure 8. Possible reaction mechanism diagram for the tribocatalytic effect.

To further confirm the involvement of hydroxyl and superoxide radicals, a radical scavenger assay was conducted (Figure 9).

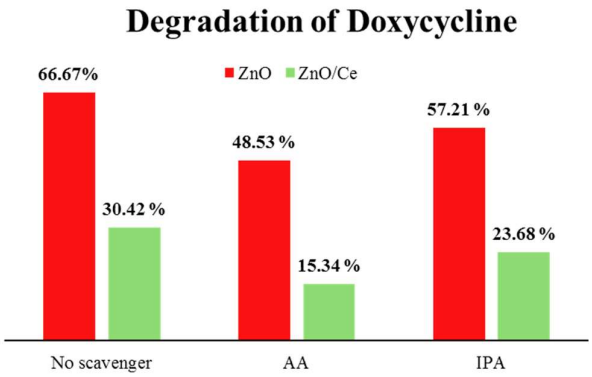


Figure 9. Effect of scavengers on doxycycline degradation in tribocatalysis process using ZnO and ZnO/Ce powders.

The contribution of superoxide ($O_2^{\bullet -}$) and hydroxyl ($OH^{\bullet}$) radicals to the degradation of doxycycline was measured by incorporating scavengers such as ascorbic acid (AA) and isopropyl alcohol (IPA), which bind to the corresponding reactive species [39–42]. As shown in Figure 9, both tribocatalyst systems responded similarly to the addition of AA and IPA. However, in the case of AA, a more pronounced inhibition was observed, indicating that the generation of the superoxide radical plays a greater role in the DC tribodegradation rate.

2.3. Tribocatalysis for Degradation of Doxycycline via Different Magnetic Stirring Speeds

ZnO and ZnO/Ce powders were employed in tribocatalytic reactions for the degradation of doxycycline (DC) at different rotational speeds: 100, 300, and 500 rpm. The mixture was continuously stirred for 24 h, during which the drug concentration progressively decreased. The tribocatalytic characteristics of ZnO and ZnO/Ce powders regarding the effect of stirring speed on the DC degradation are illustrated in Figure 10. At 100, 300, and 500 rpm, the tetracycline antibiotic was degraded by 49.2%, 66.7%, and 80.4%, respectively, in the presence of pure ZnO (Figure 10a).

In all three cases, the Ce-modified powder exhibited poorer catalytic performance for drug decomposition. An increase in magnetic stirring speed accelerated the breakdown of the tetracycline drug. The rate constant (k) increased with faster rotation speeds, leading to improved catalyst efficiency (Figure 10b). Higher values of k and a greater degree of tribodegradation (Table 1) indicate a faster elimination of doxycycline due to the enhanced excitation of electrons (e^-) and the oxidation of the organic pollutant at higher rotation speeds.

Table 1. The values of rate constants and percent of doxycycline decomposition using the tribocatalytic process.

Sample Powders	100 rpm		300 rpm		500 rpm	
	k, h^{-1}	D, %	k, h^{-1}	D, %	k, h^{-1}	D, %
ZnO	0.0296	49	0.0483	67	0.0725	80
ZnO/Ce	0.0119	24	0.0168	30	0.0352	55

The degradation of DC was tracked using UV/Vis spectroscopy, monitoring the absorbance maxima at 275 nm. The UV/Vis spectra for DC degradation using pure ZnO and ZnO/Ce at 500 rpm are shown in Figure 11.

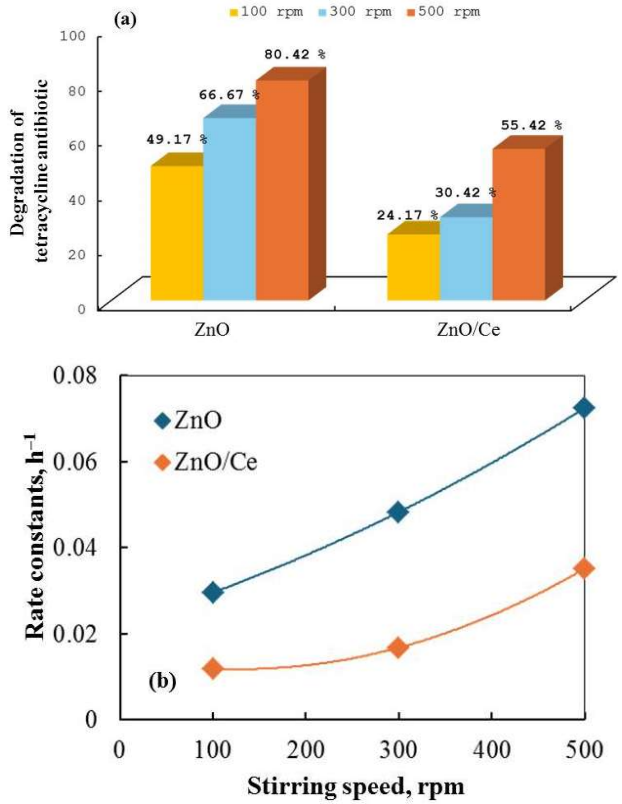


Figure 10. (**a**) Degradation of doxycycline at different rotation speeds, (**b**) relation between rate constants and different magnetic stirring speeds using ZnO and ZnO/Ce powders.

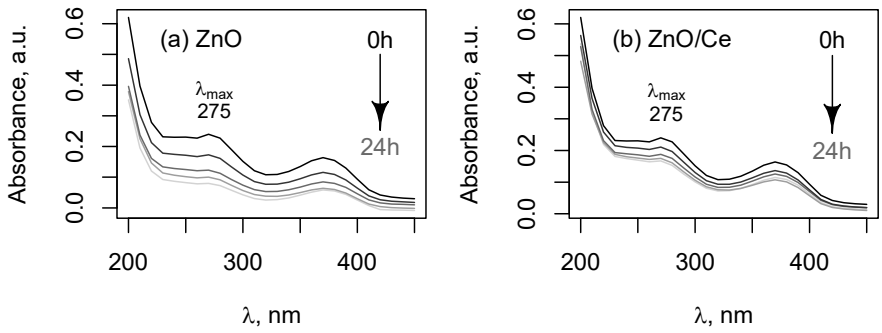


Figure 11. UV/vis spectra showing DC tribodegradation over 24 h, with measurements taken every 6 h and rotation speed at 500 rpm, using (**a**) ZnO and (**b**) ZnO/Ce. The drug absorbance peak at 275 nm (λmax) is labeled.

The tribocatalytic results at a rotation speed of 500 rpm were confirmed by Total Organic Carbon (TOC) analysis. TOC measurements were carried out to assess the degradation of doxycycline after 24 h of magnetic stirring in the dark, as shown in Figure 12. The TOC percentages for the decomposition of DC were 65.37% and 43.62% for the ZnO and ZnO/Ce powders, respectively. The TOC removal percentages of the tetracycline antibiotic were slightly lower than their decomposition rates during the tribocatalytic processes. This discrepancy was attributed to the formation of intermediate byproducts.

Compared to UV–vis spectroscopy, the TOC measurements revealed lower values of doxycycline removal. This discrepancy indicates the presence of multiple intermediate products involved in the complex multistep process of mineralization. For instance, during the drug's photocatalytic oxidation, S. Pourmoslemi identified several intermediate products [43]. When interacting with the hydroxyl and superoxide radicals generated during the catalytic process, each of these byproducts possesses a distinct oxidation potential.

Consequently, each intermediate will mineralize at a different rate, which is more easily detected during TOC analysis.

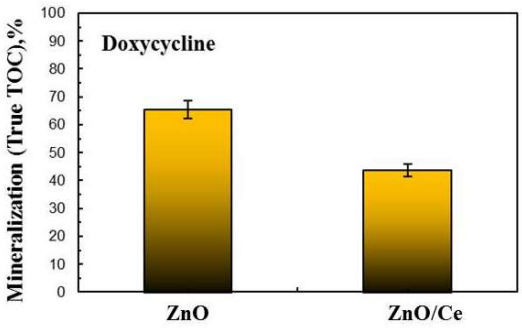


Figure 12. Histograms of TOC conversion.

3. Materials and Methods

Materials: Commercial zinc oxide powder (>99.0%), cerium nitrate hexahydrate ($Ce(NO_3)_3 \cdot 6H_2O$, >99.0%), and absolute ethanol (C_2H_5OH) were obtained from Fluka (Burlington, MA, USA).

Doxycycline (DC, $C_{22}H_{24}N_2O_8$, λ_{max} = 275 nm, Teva, Bulgaria) was selected as the model pollutant for the tribocatalytic experiments due to its widespread use and potential environmental impact. Doxycycline, a member of the tetracycline antibiotic class, is commonly used to treat various infections, including those of the skin, eyes, urinary tract, and respiratory system.

Synthesis of ZnO/Ce Powders: ZnO/Ce powders were synthesized using a simple and eco-friendly hydrothermal process. To prepare Ce-modified tribocatalysts, commercial ZnO powder and $Ce(NO_3)_3.6H_2O$ (2 mol%) were combined in a glass vessel, with ethanol added as the mixing medium. The mixture was stirred for 10 min, sonicated for 30 min, and then dried at 100 °C for 1 h to obtain the ZnO/Ce powders used in tribocatalytic testing.

Characterization Techniques: X-ray diffraction (XRD), to obtain the crystalline structure and phase composition of the as-prepared tribocatalysts, was performed on a Siemens D55 diffractometer (Karlsruhe, Germany) with CuKα radiation in the 2θ range of 25–75°. Mean crystallite dimensions and stress were evaluated through Rietveld analysis using PowderCell software, version 2.4. [44]. The surface morphology of the pure and Ce-modified ZnO was analyzed via scanning electron microscopy (SEM) on a JSM-5510 SEM (Krefeld, Germany) at an acceleration voltage of 10 kV. Energy-dispersive X-ray spectroscopy (EDX) for elemental analysis and chemical composition was performed using a Quantax 200 EDX detector (Bruker, Berlin, Germany) with a resolution of 126 eV. Transmission electron microscopy (TEM) analysis was conducted using a JEOL JEM-2100 microscope (Tokyo, Japan) at 200 kV. X-ray Photoelectron spectroscopy (XPS) was performed with an ESCALAB MkII spectrometer (Thermo Scientific, Manchester, UK) using a non-monochromated AlKα X-ray source (excitation energy: 1486.6 eV). The base pressure was 5×10^{-10} mbar, and the instrumental resolution was approximately 1 eV. Data were analyzed using SpecsLabII CasaXPS software (version 2.3.25PR1). Raman spectra were obtained using a ThunderOptics Eddu TO-ERS-532 spectrometer (Montpellier, France) with a 20× microscope objective lens and a 532 nm laser source.

Tribocatalytic Experiments: Tribocatalytic tests were conducted in a 100 mL glass beaker with a magnetic stirrer. A 50 mL solution of DC (15 ppm) in distilled water was used as the test medium. The tribocatalytic reactions were carried out at room temperature (23 ± 2 °C) in the absence of light. For each experiment, 50 mg of either pure or Ce-modified ZnO catalyst was added to the DC solution, and a PTFE-coated magnetic bar (ø 8 mm, L = 35 mm) was used for stirring. The mixture was allowed to reach adsorption equilibrium between the tribocatalysts and the DC solution by standing for 30 min without stirring. The magnetic stirrer was then activated, rotating initially at 300 rpm. Aliquots (2 mL)

of the reaction solution were periodically collected, and the tribocatalyst was separated by centrifugation at 6000 rpm. The aliquots were analyzed using UV-Vis spectroscopy in the 200–450 nm range. This procedure was repeated under different magnetic stirring conditions (100 and 500 rpm).

Control Experiments: Additional tests were conducted without catalysts and without PTFE stirring to verify that no significant removal of doxycycline occurred under these conditions.

Scavenger Assay: To identify the reactive species involved in the DC degradation, scavenger tests were performed using isopropyl alcohol (IPA) and ascorbic acid (AA) to absorb hydroxyl and superoxide radicals, respectively. Six milligrams of each scavenger were independently added to the reaction mixture to determine the contribution of these radicals to the tribocatalytic degradation process.

Total Organic Carbon (TOC) Analysis: TOC measurements of the treated dye solutions were conducted using an Elementar Vario Select TOC analyzer (Langenselbold, Germany) with a high-temperature (850 °C) catalytic oxidation method. Each sample was measured three times to determine the standard deviation.

4. Conclusions

The degradation of the tetracycline antibiotic doxycycline was successfully achieved using ZnO and ZnO/Ce powders under varying magnetic stirring speeds (100, 300, and 500 rpm) in dark conditions. The increase in rotational speed significantly enhanced the degradation rate, demonstrating that the mechanical energy generated through friction effectively excites the electrons and holes in the ZnO and ZnO/Ce catalysts. This study highlights the potential of tribocatalysis as a sustainable and energy-efficient approach for the degradation of environmental pollutants, utilizing mechanical energy from the surrounding environment to drive the breakdown of harmful substances. The findings open up new possibilities for applying tribocatalysis in environmental remediation, offering a novel pathway to reduce the impact of pharmaceutical contaminants on ecosystems.

Author Contributions: Conceptualization, N.K.; methodology, N.K.; formal analysis, N.K.; investigation, D.I., H.K. and B.I.S.; data curation, N.K.; writing—original draft preparation, N.K.; writing—review and editing, N.K. and B.I.S.; visualization, D.I., N.K., H.K. and B.I.S.; supervision, N.K. All authors have read and agreed to the published version of the manuscript.

Funding: This research received no external funding.

Data Availability Statement: Data are contained within the article.

Acknowledgments: Research equipment of distributed research infrastructure INFRAMAT, supported by the Bulgarian Ministry of Education and Science under contract D01-284/17.12.2019, was used.

Conflicts of Interest: The authors declare no conflicts of interest.

References

1. Narayanan, D.; Bhat, M.; Paul, N.; Khatri, N.; Saroliya, A. Artificial intelligence driven advances in wastewater treatment: Evaluating techniques for sustainability and efficacy in global facilities. *Desalin. Water Treat.* **2024**, *320*, 100618. [CrossRef]
2. Hamedani, E.; Abasalt, A.; Talebi, S. Application of microbial fuel cells in wastewater treatment and green energy production: A comprehensive review of technology fundamentals and challenges. *Fuel* **2024**, *370*, 131855. [CrossRef]
3. Astira, D.; Abdullah, R.; Widyanto, A.; Dharma, H.; Santoso, L.; Sulistiono, D.; Rahmawati, Z.; Gunawan, T.; Jaafar, J.; Othman, M.; et al. A recent development on core-shell-based material and their application in membranes for water and wastewater treatment. *Inorg. Chem. Commun.* **2024**, *160*, 111678. [CrossRef]
4. Dong, S.; Cui, L.; Tian, Y.; Xia, L.; Wu, Y.; Yu, J.; Bagley, D.; Sun, J.; Fan, M. A novel and high-performance double Z-scheme photocatalyst ZnO-SnO_2-Zn_2SnO_4 for effective removal of the biological toxicity of antibiotics. *J. Hazard. Mater.* **2020**, *399*, 123017. [CrossRef]
5. Yu, S.; Xie, Z.; Wu, X.; Zheng, Y.; Shi, Y.; Xiong, Z.; Zhou, P.; Liu, Y.; He, C.; Pan, Z.; et al. Review of advanced oxidation processes for treating hospital sewage to achieve decontamination and disinfection. *Chin. Chem. Lett.* **2024**, *35*, 108714. [CrossRef]
6. Ani, I.; Akpan, U.; Olutoye, M.; Hameed, B.; Egbosiuba, T. Adsorption–photocatalysis synergy of reusable mesoporous TiO_2–ZnO for photocatalytic degradation of doxycycline antibiotic. *Heliyon* **2024**, *10*, e30531. [CrossRef] [PubMed]

7. Ranjith, K.; Yildiz, Z.; Khalily, M.; Huh, Y.; Han, Y.; Uyar, T. Membrane-based electrospun poly-cyclodextrin nanofibers coated with ZnO nanograins by ALD: Ultrafiltration blended photocatalysis for degradation of organic micropollutants. *J. Membr. Sci.* **2023**, *686*, 122002. [CrossRef]
8. Mahlangu, O.; Mamba, G.; Mamba, B. A facile synthesis approach for GO-ZnO/PES ultrafiltration mixed matrix photocatalytic membranes for dye removal in water: Leveraging the synergy between photocatalysis and membrane filtration. *J. Environ. Chem. Eng.* **2023**, *11*, 110065. [CrossRef]
9. Dyshlyuk, L.; Babich, O.; Ivanova, S.; Vasilchenco, N.; Atuchin, V.; Korolkov, I.; Russakov, D.; Prosekov, A. Antimicrobial potential of ZnO, TiO_2 and SiO_2 nanoparticles in protecting building materials from biodegradation. *Int. Biodeterior. Biodegrad.* **2020**, *146*, 104821. [CrossRef]
10. Zhang, L.; Li, X.; Chen, S.; Guan, J.; Guo, Y.; Yu, W. 3D chitosan/GO/ZnO hydrogel with enhanced photocorrosion-resistance and adsorption for efficient removal of typical water-soluble pollutants. *Catal. Commun.* **2023**, *176*, 106627. [CrossRef]
11. Roy, N.; Kannabiran, K.; Mukherjee, A. Integrated adsorption and photocatalytic degradation based removal of ciprofloxacin and sulfamethoxazole antibiotics using Fc@rGO-ZnO nanocomposite in aqueous systems. *Chemosphere* **2023**, *333*, 138912. [CrossRef] [PubMed]
12. Xing, L.; Haddao, K.; Emami, N.; Nalchifard, F.; Hussain, W.; Jasem, H.; Dawood, A.; Toghraie, D.; Hekmatifar, M. Fabrication of HKUST-1/ZnO/SA nanocomposite for Doxycycline and Naproxen adsorption from contaminated water. *Sustain. Chem. Pharm.* **2022**, *29*, 100757. [CrossRef]
13. Wang, X.; Lin, X.; Yu, D. Metal-containing covalent organic framework: A new type of photo/electrocatalyst. *Rare Met.* **2022**, *41*, 1160–1175. [CrossRef]
14. Feng, A.; Yang, M.; Zhang, Z.; Xia, H.; Jin, W.; Shen, B.; Hu, Y.; Li, Q. Electrocatalytic hydrogen evolution coupled with dye hydrogenation reactions for sustainable wastewater treatment using transition-metal (Fe, Co, Ni, Cu) nanoparticles with ZnO nanowire supports. *Chem. Eng. J.* **2024**, *496*, 153751. [CrossRef]
15. Chen, L.; Li, C.; Xu, B.; Xing, B.; Yi, G.; Huang, G.; Zhang, C.; Liu, J. Microbial degradation of organic pollutants in groundwater related to underground coal gasification. *Energy Sci. Eng.* **2019**, *7*, 2098–2111. [CrossRef]
16. Liu, J.; Liu, J.; Zhu, X.; Ruan, Q.; Li, D.; Huang, C.; Peng, Q.; Zhu, S.; Gao, X.; Wang, B.; et al. Halogen-doped ultrathin Bi2WO6 for promoted separation of photogenerated carriers and efficient photocatalysis. *Colloids Surf. A* **2024**, *695*, 134113. [CrossRef]
17. Wang, Z.; Wang, J.; Zhang, J.; Dai, K. Overall utilization of photoexcited charges for simultaneous photocatalytic redox reactions. *Acta Phys. Chim. Sin.* **2023**, *39*, 2209037. [CrossRef]
18. Li, X.; Wang, Q.; Sun, Y.; Sun, S.; Ge, L. Photogenerated charge carriers' regulation strategies: Structure design, mechanism, and characterization technology. *Int. J. Hydrogen Energy* **2024**, *69*, 1341–1365. [CrossRef]
19. Ali, Y.; Azzouz, A.; Ahrouch, M.; Lamaoui, A.; Raza, N.; Lahcen, A. Molecular imprinting technology for next-generation water treatment via photocatalysis and selective pollutant adsorption. *J. Environ. Chem. Eng.* **2024**, *12*, 112768.
20. Lei, H.; Wu, M.; Mo, F.; Ji, S.; Dong, X.; Wu, Z.; Gao, J.; Yang, Y.; Jia, Y. Tribo-catalytic degradation of organic pollutants through bismuth oxyiodate triboelectrically harvesting mechanical energy. *Nano Energy* **2020**, *78*, 105290. [CrossRef]
21. Gaur, A.; Moharana, A.; Porwal, C.; Chauhan, V.; Vaish, R. Degradation of organic dyes by utilizing $CaCu_3Ti_4O_{12}$ (CCTO) nanoparticles via tribocatalysis process. *J. Ind. Eng. Chem.* **2024**, *129*, 341–351. [CrossRef]
22. Zhang, L.; Ding, W.; Qiu, J.; Jin, H.; Ma, H.; Li, Z.; Cang, D. Modeling and optimization study on sulfamethoxazole degradation by electrochemically activated persulfate process. *J. Clean. Prod.* **2018**, *197*, 297–305. [CrossRef]
23. Xiong, H.; Zou, D.; Zhou, D.; Dong, S.; Wang, J.; Rittmann, B. Enhancing degradation and mineralization of tetracycline using intimately coupled photocatalysis and biodegradation (ICPB). *Chem. Eng. J.* **2017**, *316*, 7–14. [CrossRef]
24. Klauson, D.; Poljakova, A.; Pronina, N.; Krichevskaya, M.; Moiseev, A.; Dedova, T.; Preis, S. Aqueous photocatalytic oxidation of doxycycline. *J. Adv. Oxid. Technol.* **2013**, *16*, 234–243. [CrossRef]
25. Boro, B.; Samdarshi, B.; Rajbongshi, S. Synthesis and fabrication of TiO_2–ZnO nanocomposite based solid state dye sensitized solar cell. *J. Mater. Sci. Mater. Electron.* **2016**, *27*, 9929–9940. [CrossRef]
26. Bolobajev, J.; Trapido, M.; Goi, A. Effect of iron ion on doxycycline photocatalytic and Fenton-based autocatatalytic decomposition. *Chemosphere* **2016**, *153*, 220–226. [CrossRef]
27. Hu, X.; Zhou, K.; Chen, B.; Chang, C. Graphene/TiO_2/ZSM-5 composites synthesized by mixture design were used for photocatalytic degradation of oxytetracycline under visible light: Mechanism and biotoxicity. *Appl. Surf. Sci.* **2016**, *362*, 329–334. [CrossRef]
28. Ada, K.; Gökgöz, M.; Önal, M.; Sarıkaya, Y. Preparation and characterization of a ZnO powder with the hexagonal plate particles. *Powder Technol.* **2008**, *181*, 285–291. [CrossRef]
29. Kumar, S.; Kavitha, R. Lanthanide ions doped ZnO based photocatalysts. *Sep. Purif. Technol.* **2021**, *274*, 118853. [CrossRef]
30. Eaimsumang, S.; Wongkasemjit, S.; Pongstabodee, S.; Smith, S.M.; Ratanawilai, S.; Chollacoop, N.; Luengnaruemitchai, A. Effect of synthesis time on morphology of CeO_2 nanoparticles and Au/CeO_2 and their activity in oxidative steam reforming of methanol. *J. Rare Earths* **2019**, *37*, 819–828. [CrossRef]
31. Qu, G.; Fan, G.; Zhou, M.; Rong, X.; Li, T.; Zhang, R.; Sun, J.; Chen, D. Graphene-Modified ZnO Nanostructures for Low-Temperature NO_2 Sensing. *ACS Omega* **2019**, *4*, 4221–4232. [CrossRef]
32. Zhao, S.; Shen, Y.; Li, A.; Chen, Y.; Gao, S.; Liu, W.; Wei, D. Effects of rare earth elements doping on gas sensing properties of ZnO nanowires. *Ceram. Int.* **2021**, *47*, 24218–24226. [CrossRef]

33. Zhang, Q.; Zhao, X.; Duan, L.; Shen, H.; Liu, R. Controlling oxygen vacancies and enhanced visible light photocatalysis of CeO_2/ZnO nanocomposites. *J. Photochem. Photobiol. A* **2020**, *392*, 112156. [CrossRef]
34. Peleš, A.; Pavlović, V.P.; Filipović, S.; Obradović, N.; Mančić, L.; Krstić, J.; Mitrić, M.; Vlahović, B.; Rašić, G.; Kosanović, D.; et al. Structural investigation of mechanically activated ZnO powder. *J. Alloys Compd.* **2015**, *648*, 971–979. [CrossRef]
35. Xu, Y.; Yin, R.; Zhang, Y.; Zhou, B.; Sun, P.; Dong, X. Unveiling the Mechanism of Frictional Catalysis in Water by $Bi_{(12)}TiO_{(20)}$: A Charge Transfer and Contaminant Decomposition Path Study. *Langmuir* **2022**, *38*, 14153–14161. [CrossRef] [PubMed]
36. Ma, J.; Wu, Z.; Luo, W.; Zheng, Y.; Jia, Y.; Wang, L.; Huang, H. High pyrocatalytic properties of pyroelectric $BaTiO_3$ nanofibers loaded by noble metal under roomtemperature thermal cycling. *Ceram. Int.* **2018**, *44*, 21835–21841. [CrossRef]
37. Al Abri, R.; Al Marzouqi, F.; Kuvarega, A.T.; Meetani, M.A.; Al Kindy, S.M.Z.; Karthikeyan, S.; Kim, Y.; Selvaraj, R. Nanostructured cerium-doped ZnO for photocatalytic degradation of pharmaceuticals in aqueous solution. *J. Photochem. Photobiol. A* **2019**, *384*, 112065. [CrossRef]
38. Lei, H.; Cui, X.; Jia, X.; Qi, J.; Wang, Z.; Chen, W. Enhanced Tribocatalytic Degradation of Organic Pollutants by ZnO Nanoparticles of High Crystallinity. *Nanomaterials* **2023**, *13*, 46. [CrossRef]
39. Xu, X.; Jia, Y.; Xiao, L.; Wu, Z. Strong vibration-catalysis of ZnO nanorods for dye wastewater decolorization via piezo-electrochemical coupling. *Chemosphere* **2018**, *193*, 1143–1148. [CrossRef]
40. Wang, Y.; Shen, S.; Liu, M.; He, G.; Li, X. Enhanced tribocatalytic degradation performance of organic pollutants by $Cu_{1.8}S/CuCo_2S_4$ p-n junction. *J. Colloid Interface Sci.* **2024**, *655*, 187–198. [CrossRef]
41. Zhao, J.; Dang, Z.; Muddassir, M.; Raza, S.; Zhong, A.; Wang, X.; Jin, J. A New Cd(II)-Based Coordination Polymer for Efficient Photocatalytic Removal of Organic Dyes. *Molecules* **2023**, *28*, 6848. [CrossRef]
42. Xiang, R.; Zhou, C.; Liu, Y.; Qin, T.; Li, D.; Dong, X.; Muddassir, M.; Zhong, A. A new type Co(II)-based photocatalyst for the nitrofurantoin antibiotic degradation. *J. Mol. Struct.* **2024**, *1312*, 138501. [CrossRef]
43. Pourmoslemi, S.; Mohammadi, A.; Kobarfard, F.; Amini, M. Photocatalytic removal of doxycycline from aqueous solution using ZnO nano-particles: A comparison between UV-C and visible light. *Water Sci. Technol.* **2016**, *74*, 1658–1670. [CrossRef] [PubMed]
44. Kraus, W.; Nolze, G. POWDER CELL—A program for the representation and manipulation of crystal structures and calculation of the resulting X-ray powder patterns. *J. Appl. Crystallogr.* **1996**, *29*, 301–303. [CrossRef]

Disclaimer/Publisher's Note: The statements, opinions and data contained in all publications are solely those of the individual author(s) and contributor(s) and not of MDPI and/or the editor(s). MDPI and/or the editor(s) disclaim responsibility for any injury to people or property resulting from any ideas, methods, instructions or products referred to in the content.